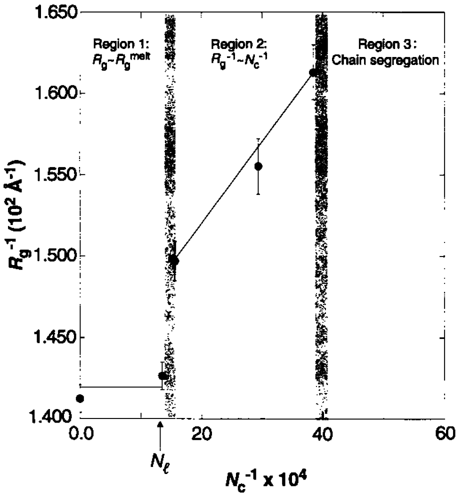

Fig. 3. Plot of the variation of R_g^{-1} with N_c^{-1}.

a systematic decrease in R_g is observed as a function of the cross-link density. The onset of region 2 appears to occur when the mesh size of the network decreases below the length of the linear chain ($N_c \leq N_\ell$). The length of the linear chains is indicated by an arrow on the abscissa in Fig. 3. In this regime, the scaling of the form predicted by Eq. 3 is observed as expected if the cross-link points are acting as random obstacles influencing the R_g of the linear chain. In region 3, the mesh size of the network is much smaller than the length of the linear chain ($N_c \ll N_\ell$), and segregation of the linear chains is observed. This segregation is clear from the non-Gaussian scattering (nonlinear) behavior observed in Fig. 2. Region 3 corresponds to a collapsed state of the polymer chain.

Although the experiments presented here cannot determine the detailed shape of the linear chains in these regimes, it is clear that the shape cannot be described by individual, isolated Gaussian chains. The gray bands in Fig. 3 show the approximate demarcation between the regions, but more experiments are needed to determine the exact location of these transitions. The segregation of the linear chains for the highest cross-link densities was surprising, as we expected the mixtures to remain single phase because of the very low concentration of linear polymer.

The contraction of R_g can be normalized to the value found in the uncross-linked melt. The ratio of R_g to the unperturbed value of R_g^0 is termed the expansion factor, α. The change in the value of α observed here (about 15%) for the collapse of the linear chain (see Table 1) is comparable to that found in studies of the collapse transition of linear polystyrene in dilute solution (*27–30*).

The collapse of the chains observed here for matrices with high cross-link density implies that the size of polymer chains in confined environments may deviate significantly from the unperturbed dimensions expected in the melt. These effects should cause changes in the dynamics of polymer chains from what would be expected for problems such as gel electrophoresis and reptation through a network.

REFERENCES AND NOTES

1. P. G. de Gennes, *J. Chem. Phys.* **53**, 572 (1971).
2. E. F. Cassasa, *Macromolecules* **9**, 182 (1976).
3. B. Lee and H. Nakanishi, *Phys. Rev. Lett.* **63**, 2819 (1989).
4. J. L. Anderson and J. A. Quinn, *Biophys. J.* **14**, 130 (1974).
5. X. Zheng *et al.*, *Macromolecules* **26**, 6431 (1993).
6. J. M. Deutsch, *Science* **240**, 922 (1988).
7. F. Brochard and P. G. de Gennes, *J. Chem. Phys.* **67**, 52 (1977).
8. M. Antonietti and H. Sillescu, *Macromolecules* **18**, 1162 (1985).
9. K. Shull *et al.*, *ibid.* **24**, 505 (1991).
10. W. L. Wu and L. Jong, *Polymer* **34**, 2357 (1993).
11. F. Boué, B. Farnoux, J. Bastide, *Europhys. Lett.* **1**, 637 (1986).
12. D. Thirumalai, *Phys. Rev. A* **37**, 269 (1988).
13. B. Duplantier, *ibid.* **38**, 3647 (1988).
14. M. Muthukumar, *J. Chem. Phys.* **90**, 4594 (1989).
15. J. F. Douglas, *Macromolecules* **21**, 3515 (1988).
16. S. F. Edwards and M. Muthukumar, *J. Chem. Phys.* **89**, 2435 (1988).
17. A. Baumgärtner and M. Muthukumar, *ibid.* **87**, 3082 (1987).
18. J. D. Honeycutt and D. Thirumalai, *ibid.* **90**, 4542 (1989).
19. D. Gersappe, J. M. Deutsch, M. Olvera de la Cruz, *Phys. Rev. Lett.* **66**, 731 (1991).
20. K. Dusek and W. Prins, *Adv. Polym. Sci.* **6**, 1 (1969).
21. Equation 3 represents a scaling relation and is used to convey the simplest form expected for the variation of R_g^{-1} with N_c^{-1}. Equation 3 could have been written as

$$1/R = 1/R_g^0 + K/N_c$$

where R_g^0 is the unperturbed radius of gyration of the linear chain in the absence of cross-links and K is a proportionality constant.
22. R. M. Briber and B. J. Bauer, *Macromolecules* **24**, 1899 (1991).
23. H. J. Prask, M. Rowe, J. J. Rush, I. G. Schroder, *J. Res. Natl. Inst. Stand. Technol.* **98**, 1 (1993).
24. Certain equipment is identified in this report in order to adequately specify the experimental details. Such identification does not imply recommendation by NIST nor does it imply that the materials are necessarily the best available for the purpose.
25. B. H. Zimm, *J. Chem. Phys.* **16**, 1093 (1948).
26. K. Mori, H. Tanaka, H. Hasegawa, T. Hashimoto, *Polymer* **30**, 1389 (1989).
27. A. Z. Akcasu and C. C. Han, *Macromolecules* **12**, 276 (1979).
28. B. Chu, I. H. Park, Q.-W. Wang, C. Wu, *ibid.* **20**, 2833 (1987).
29. P. Vidakovic and R. Rondelelz, *ibid.* **17**, 418 (1984).
30. M. Nierlich, J. P. Cotton, B. Farnoux, *J. Chem. Phys.* **69**, 1379 (1978).
31. Supported in part by the Donors of the Petroleum Research Fund, administered by the American Chemical Society. One of the authors (X.L.) was supported under a cooperative research agreement between the University of Maryland and the Reactor Radiation Division at NIST. We also acknowledge the support of NIST, U.S. Department of Commerce, in providing the neutron research facilities used in this work.

10 November 1994; accepted 2 February 1995

High-Temperature Molecular Magnets Based on Cyanovanadate Building Blocks: Spontaneous Magnetization at 230 K

William R. Entley and Gregory S. Girolami*

The molecular-based magnetic materials $Cs_2Mn^{II}[V^{II}(CN)_6]$ (**1**) and $(Et_4N)_{0.5}Mn_{1.25}[V(CN)_5]\cdot 2H_2O$ (**2**) (where Et is ethyl) were prepared by the addition of manganese(II) triflate to aqueous solutions of the hexacyanovanadate(II) ion at 0°C. Whereas **1** crystallizes in a face-centered cubic lattice, **2** crystallizes in a noncubic space group. The cesium salt (**1**) has features characteristic of a three-dimensional ferrimagnet with a Néel transition at 125 kelvin. The tetraethylammonium salt (**2**) also behaves as a three-dimensional ferrimagnet with a Néel temperature of 230 kelvin; only two other molecular magnets have higher magnetic ordering temperatures. Saturation magnetization measurements indicate that in both compounds the V^{II} and high-spin Mn^{II} centers are antiferromagnetically coupled. Both **1** and **2** exhibit hysteresis loops characteristic of soft magnets below their magnetic phase-transition temperatures. The high magnetic ordering temperatures of these cyano-bridged solids confirm that the incorporation of early transition elements into the lattice promotes stronger magnetic coupling by enhancing the backbonding into the cyanide π^* orbitals.

In the last few years, there has been considerable interest in the preparation and properties of "molecular magnets" (*1–3*). Although a wide variety of such materials is now known, most exhibit long-range cooperative magnetic behavior only when they are cooled to rather low temperatures, often well below 30 K (*4–12*). For example, the one-dimensional (1D) materials $[Mn(C_5Me_5)_2]$ (TCNE) (Me = methyl) (*7*), $[Mn(F_5benz)_2]_2(nitMe)$ (*10*), and $MnCu(pbaOH)\cdot 2H_2O$ (*6*) have magnetic ordering temperatures T_N of 8.8, 24, and

---

School of Chemical Sciences and Frederick Seitz Materials Research Laboratory, University of Illinois at Urbana-Champaign, 505 South Mathews Avenue, Urbana, IL 61801, USA.

*To whom correspondence should be addressed.

30 K, respectively (*13*). In most cases, these low values are consequences of the low dimensionalities of the lattices: magnetic interactions between 1D chains are weak because they must propagate through space rather than through bonds (*14, 15*). Recently, however, Miller and co-workers have reported an amorphous solid of approximate stoichiometry $V(TCNE)_2 \cdot \frac{1}{2} CH_2Cl_2$, which is the first example of a molecular material that is magnetic at room temperature (*16*). The high magnetic ordering temperatures T_N of this solid undoubtedly reflects the presence of strong 3D interactions among the adjacent spin centers (*15, 16*). Unfortunately, the discovery of $V(TCNE)_2 \cdot \frac{1}{2} CH_2Cl_2$ has not yet led to the development of a general route to molecular magnets with high T_N.

One potential general route to the synthesis of molecular magnets with T_N above 300 K is to make analogs of Prussian blue. Prussian blue is a mixed-valent cyanoferrate of stoichiometry $Fe^{III}{}_4[Fe^{II}(CN)_6]_3 \cdot xH_2O$ in which iron(II) and iron(III) centers form a cubic lattice linked by cyanide ligands. Prussian blue has a rather low magnetic ordering temperature of 5.6 K: The paramagnetic Fe^{3+} ions are weakly interacting because they are separated by intervening diamagnetic Fe^{2+} centers (*17*). In contrast, analogs of Prussian blue in which all of the centers are paramagnetic are especially attractive as candidates for new molecular magnets for several reasons: (i) the linear M–CN–M′ bridges promote the formation of strong magnetic interactions between adjacent spin centers, (ii) the solids can be easily prepared at room temperature from well-characterized cyanometallate building blocks, and (iii) a wide range of metals with different spin states and oxidation states can be substituted into the lattice (*18, 19*). These features allow considerable control over the nature and the magnitude of the local magnetic exchange interactions.

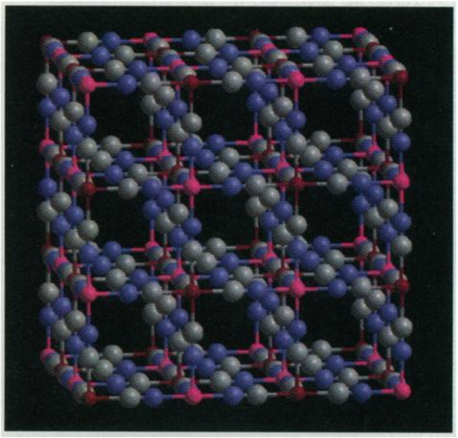

Fig. 1. Structure of $Cs_2Mn^{II}[V^{II}(CN)_6]$ (**1**). Each cube interior is occupied by a Cs^+ ion. The maroon spheres represent V^{II} centers (C_6 coordination environments), and the pink spheres represent Mn^{II} centers (N_6 coordination environments).

The magnetic properties of a number of Prussian blue analogs have been described (*18, 20–23*), and the nature of the exchange interactions has been discussed (*24*); the antiferromagnetic interactions, which are thought to propagate principally through the empty π^* orbitals of the cyanide ligand, are generally dominant (*18, 20, 21*). Because T_N is directly related to the magnitude of the spin coupling between adjacent metal centers (*25*), it should be possible to increase T_N in Prussian blue analogs by increasing the extent of π-backbonding into the cyanide π^* orbitals. One way to accomplish this is to substitute into the structure metals that have high-energy t_{2g} orbitals. In particular, it might be possible to prepare solids with T_N near 300 K by substituting low-valent V or Ti centers into a cyanide-bridged 3D lattice, but to our knowledge no such materials have been reported. We describe herein the synthesis, characterization, and magnetic properties of V-containing analogs of Prussian blue; one of these solids exhibits spontaneous magnetization at 230 K. The cyanovanadate reagents we have used as molecular building blocks are the potassium and tetraethylammonium salts of the hexacyanovanadate(II) ion: $K_4[V(CN)_6]$ (*26*) and $(NEt_4)_4[V(CN)_6]$ (Et = ethyl) (*27*).

Addition of $Mn(OSO_2CF_3)_2(CH_3CN)_2$ (*28*) to an aqueous solution of $CsOSO_2CF_3$ (*28*) and $K_4[V(CN)_6]$ under argon at 0°C yields an air-sensitive green solid (*29*) of stoichiometry $Cs_2Mn^{II}[V^{II}(CN)_6]$ (**1**) (Fig. 1). The infrared (IR) spectrum of this material shows a strong $\nu_{C\equiv N}$ stretch at 2097 cm^{-1} and a shoulder at 2062 cm^{-1}. The frequency of the former band is consistent with the presence of bridging cyanide groups that are C-bound to V^{II} and N-bound to Mn^{II} (*19*). The shoulder at 2062 cm^{-1} suggests that there is some disorder in the cyanide positions (*18, 22, 30*); for example, some of the bridging cyanide ligands are C-bound to Mn^{II} and N-bound to V^{II}. The powder x-ray diffraction (XRD) pattern of **1** is able to be indexed to a face-centered-cubic (fcc) lattice with a = 10.66 Å; no extraneous peaks are present in the XRD pattern. This information and the magnetic studies below show that the lattice of **1** consists principally of alternating V^{II} ($t_{2g}{}^3$) and Mn^{II} ($t_{2g}{}^3e_g{}^2$) centers bridged by cyanide ligands; the Cs^+ cations occupy the cube "interiors" described by the cyanide-bridged lattice. The near-IR spectrum shows no intervalence transfer band, which indicates that electron transfer between the V^{II} and Mn^{II} centers is not occurring.

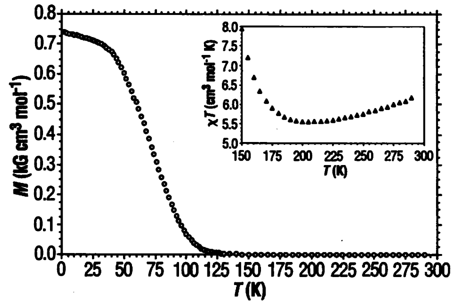

Fig. 2. Temperature dependence of the magnetization M per formula unit of $Cs_2Mn^{II}[V^{II}(CN)_6]$ (**1**) in an applied magnetic field H of 25 G. The inset shows the minimum observed at 200 K in a plot of χT versus T.

The room-temperature value of χT is 6.2(3) cm^3 K mol^{-1} (where χ is the magnetic susceptibility and T is the temperature; numbers in parentheses are standard errors in the last digit); this value closely agrees with the value of 6.3 cm^3 K mol^{-1} calculated for a thermally random mixture of equal populations of S = 5/2 and S = 3/2 spin centers. As the sample is cooled, χT gradually decreases and reaches a minimum near 200 K (Fig. 2, inset); a fit of the data to the Curie-Weiss equation $\chi = C/(T - \theta)$ (where C is a constant) over the temperature range from 290 to 265 K yields a Weiss constant, θ, of −250 K. The minimum in the curve of χT versus T (*4*) and the negative Weiss constant indicate that the adjacent spin centers in **1** are antiferromagnetically coupled.

At lower temperatures, **1** becomes strongly magnetic, as shown by the rapid increase in the magnetization below 125 K (Fig. 2). Fitting the high-temperature reciprocal susceptibility of **1** to a hyperbola based on Néel's theory (*31*) confirms that T_N is 125 K. We established the antiferromagnetic nature of the interaction between the adjacent V^{II} and Mn^{II} centers quantitatively by measuring the field dependence of the magnetization of **1** at 4.5 K (Fig. 3). The saturation magnetization at 70 kG is 1.34(6) × 10^4 G cm^3 mol^{-1}; this value is consistent with the calculated

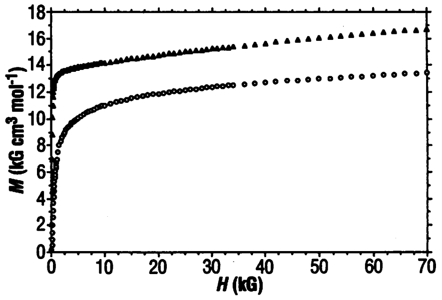

Fig. 3. Field dependence of the magnetization at 4.5 K of $Cs_2Mn^{II}[V^{II}(CN)_6]$ (**1**) (○) and $(Et_4N)_{0.5}Mn_{1.25}[V(CN)_5] \cdot 2H_2O$ (**2**) (△).

value of 1.12×10^4 G cm^3 mol^{-1} expected for equal populations of antiferromagnetically coupled V^{II} and high-spin Mn^{II} centers (*32*) but inconsistent with the value of 4.47×10^4 G cm^3 mol^{-1} expected for ferromagnetically coupled centers.

Treatment of $(NEt_4)_4[V(CN)_6]$ with $Mn(OSO_2CF_3)_2(CH_3CN)_2$ in the absence of Cs^+ triflate yields a yellow compound tentatively formulated on the basis of microanalytical data as $(Et_4N)_{0.5}Mn_{1.25}[V(CN)_5]\cdot 2H_2O$ (**2**) (*29*); the stoichiometry varies slightly depending on reaction conditions, and the possibility that the solid is a mixture of distinct species cannot be ruled out. Besides bands that are a result of the $(NEt_4)^+$ cation, the IR spectrum of **2** contains features attributable to the cyanide groups at 2094 and 2079 cm^{-1} with a shoulder at 2066 cm^{-1}, and clearly shows that there are no terminal vanadyl species present. The frequencies of the ν_{CN} stretching bands are characteristic of bridging cyanide ligands (*19*), but evidently several different cyanide environments are present in **2**. There is no intervalence electron transfer band in the near-IR spectrum.

Unlike the behavior seen for **1**, the curve of χT versus T for **2** exhibits no minimum as the sample is cooled from 350 K; instead, χT gradually increases as the temperature decreases (Fig. 4, inset). Most interesting, however, is the T_N value of 230 K (corresponding to the sharp rise in the magnetization as the sample is cooled; see Fig. 4). Among reported molecular magnetic materials, only two exhibit higher T_N values: the vanadium-TCNE compound of Miller and co-workers (*16*) (T_N estimated to be ~400 K) and the cyanochromate $[Cr_5(CN)_{12}]\cdot 10H_2O$ compound of Verdaguer and co-workers (*18*) (T_N = 240 K).

The lack of a minimum in the curve of χT versus T for **2** suggests at first glance that the V^{II} and Mn^{II} spin centers are ferromagnetically coupled, but this conclusion is contradicted by the saturation magnetization: The experimental value of $1.7(1) \times 10^4$ G cm^3 mol^{-1} at 4.5 K (Fig. 3) differs significantly from the saturation magnetization of 5.17×10^4 G cm^3 mol^{-1} calculated by assuming that the metal centers in **2** are ferromagnetically coupled but it agrees closely with the value of 1.81×10^4 G cm^3 mol^{-1} calculated for antiferromagnetic coupling (*32*). The lack of a minimum in the curve of χT versus T for **2** probably means that the minimum lies above the 350 K limit of our data (this being near the temperature at which **2** begins to decompose). In other words, the antiferromagnetic interaction between the V^{II} and Mn^{II} centers is strong enough to depopulate states of high spin multiplicity even at 350 K, and χT continuously increases as the sample is cooled because short-range order keeps the uncompensated moments parallel to each other (*9–11*). The magnetic data for **2** are thus consistent with bulk ferrimagnetic behavior below its T_N of 230 K (*33, 34*).

The powder XRD pattern clearly shows that **2** is polycrystalline but that it does not adopt a fcc structure like **1**. The noncubic XRD pattern and the unusual ratio of CN^- to V both suggest that the structure of **2** is more complex than that of **1**; further studies need to be undertaken to determine its 3D structure. Interestingly, Babel has shown that attempts to substitute cations larger than Cs^+ into the Prussian blue lattice usually give rise instead to lower dimensional structures with substantially decreased magnetic phase-transition temperatures (*20*). Even though the large $(NEt_4)^+$ cations evidently prevent the adoption of the cubic Prussian blue structure, the high value of T_N suggests that the structure of **2** still consists of a 3D array of interacting spin centers.

Both **1** and **2** exhibit hysteresis below their T_N values. For **2**, the coercive field is nearly zero at 220 K, although the magnetization as a function of external field strength clearly exhibits an S-shaped curve characteristic of hysteretic behavior (Fig. 5). As the temperature is lowered, the coercive field of the material increases and reaches a limiting value of ~24 G below 50 K. The coercive field for **1** at 10 K is only slightly larger: ~100 G (*35*). The small values of the coercive fields for **1** and **2** lend support to our contention that the metal centers present in these solids are magnetically isotropic V^{II} and high-spin Mn^{II} ions. In contrast, Prussian blue analogs that contain magnetically anisotropic metal centers exhibit considerably larger coercive fields (*5, 22*).

The V-based Prussian blue analogs that we have prepared confirm our expectation that substitution of early transition metals into the lattice should lead to higher T_N values. It is especially instructive to compare the behavior of $Cs_2Mn^{II}[V^{II}(CN)_6]$ (**1**) with that of two other isoelectronic and isostructural species, $CsMn^{II}[Cr^{III}(CN)_6]\cdot H_2O$ (*20*) and $Mn^{II}[Mn^{IV}(CN)_6]\cdot xH_2O$ (*21*). All three compounds have d^5 Mn^{II} centers in the weak ligand-field sites (N_6 coordination environments) and d^3 metal centers in the strong ligand-field sites (C_6 coordination environments); the principal difference is that the energies of the t_{2g} orbitals in the latter sites decrease as the metal changes from V^{II} to Cr^{III} to Mn^{IV}. The relative magnetic-ordering temperatures of 125, 90, and 49 K for $Cs_2Mn^{II}[V^{II}(CN)_6]$, $CsMn^{II}[Cr^{III}(CN)_6]\cdot H_2O$, and $Mn^{II}[Mn^{IV}(CN)_6]\cdot xH_2O$, respectively, clearly show that incorporation of transition metals with higher energy t_{2g} orbitals into the strong ligand-field sites leads to higher magnetic phase-transition temperatures. As the back-bonding with the cyanide π^* orbitals becomes more effective, the coupling between the adjacent spin centers increases. These two V-based molecular magnets represent an important step in the design of molecular magnets with high T_N. Through judicious choice of cations and metal centers, T_N values above 300 K should be possible.

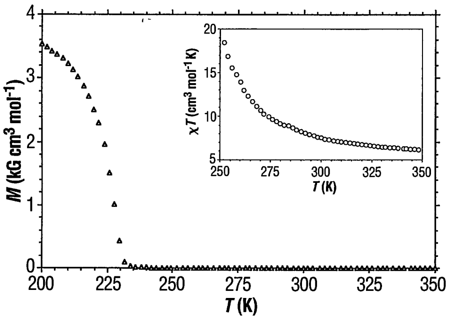

Fig. 4. Temperature dependence of the magnetization *M* per formula unit of $(Et_4N)_{0.5}Mn_{1.25}[V(CN)_5]\cdot 2H_2O$ (**2**) in an applied magnetic field *H* of 50 G. The inset shows the gradual increase in χT as the sample is cooled below 350 K.

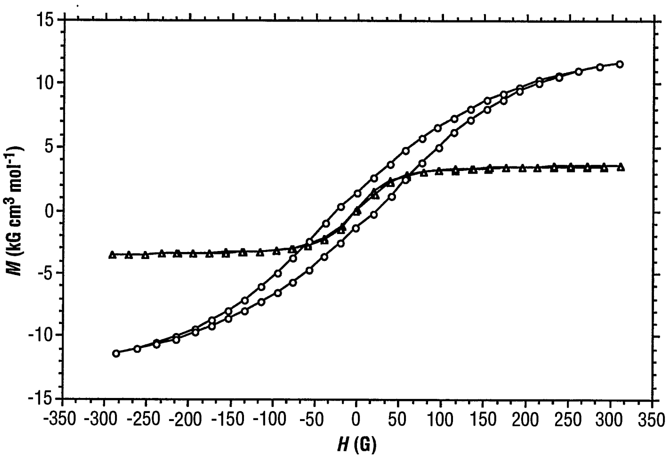

Fig. 5. Hysteresis loops of $(Et_4N)_{0.5}Mn_{1.25}[V(CN)_5]\cdot 2H_2O$ (**2**) at 220 K (△) and 50 K (○).

REFERENCES AND NOTES

1. J. S. Miller and A. J. Epstein, *Angew. Chem. Int. Ed. Engl.* **33**, 385 (1994).
2. O. Kahn, *Molecular Magnetism* (VCH, New York, 1993).
3. D. Gatteschi, O. Kahn, J. S. Miller, F. Palacio, Eds., *Magnetic Molecular Materials* (Kluwer, Dordrecht, Netherlands, 1991).
4. H. O. Stumpf, L. Ouahab, Y. Pei, P. Bergerat, O. Kahn, *J. Am. Chem. Soc.* **116**, 3866 (1994).
5. H. O. Stumpf *et al.*, *Chem. Mater.* **6**, 257 (1994).
6. K. Nakatani *et al.*, *Inorg. Chem.* **30**, 3977 (1991).
7. G. T. Yee *et al.*, *Adv. Mater.* **3**, 309 (1991).
8. J. S. Miller *et al.*, *J. Am. Chem. Soc.* **109**, 769 (1987).
9. A. Caneschi, D. Gatteschi, A. Lirzin, *J. Mat. Chem.* **4**, 319 (1994).
10. A. Caneschi, D. Gatteschi, J. P. Renard, P. Rey, R. Sessoli, *J. Am. Chem. Soc.* **111**, 785 (1989).
11. A. Caneschi, D. Gatteschi, P. Rey, R. Sessoli, *Inorg. Chem.* **27**, 1756 (1988).
12. P.-M. Allemand *et al.*, *Science* **253**, 301 (1991).
13. Abbreviations used are as follows: Me = methyl; TCNE = tetracyanoethylenide; F_5benz = pentafluorobenzoate; nitMe = 2-methyl-4,4,5,5-tetramethyl-4,5-dihydro-1*H*-imidazoyl-1-oxy-3-oxide; pbaOH = 2-hydroxy-1,3-propanediylbis(oxamato).
14. H. O. Stumpf, L. Ouahab, Y. Pei, D. Grandjean, O. Kahn, *Science* **261**, 447 (1993).
15. H. O. Stumpf, Y. Pei, O. Kahn, J. Sletten, J. P. Renard, *J. Am. Chem. Soc.* **115**, 6738 (1993).
16. J. M. Manriquez, G. T. Yee, R. S. McLean, A. J. Epstein, J. S. Miller, *Science* **252**, 1415 (1991).
17. F. Herren, P. Fischer, A. Ludi, W. Hälg, *Inorg. Chem.* **19**, 956 (1980).
18. T. Mallah, S. Thiébaut, M. Verdaguer, P. Veillet, *Science* **262**, 1554 (1993).
19. A. Ludi and H. U. Güdel, *Struct. Bonding (Berlin)* **14**, 1 (1973).
20. D. Babel, *Comments Inorg. Chem.* **5**, 285 (1986).
21. R. Klenze, B. Kanellakopulos, G. Trageser, H. H. Eysel, *J. Chem. Phys.* **72**, 5819 (1980).
22. W. R. Entley and G. S. Girolami, *Inorg. Chem.* **33**, 5165 (1994).
23. R. M. Bozorth, H. J. Williams, D. E. Walsh, *Phys. Rev.* **103**, 572 (1956).
24. For a Prussian blue structure, magnetic orbitals on adjacent metal centers M and M′ will contribute to the superexchange as follows: e_g–e_g and t_{2g}–t_{2g} combinations (if present) have nonzero overlap and give rise to antiferromagnetic contributions; e_g–t_{2g} combinations (if present) have zero overlap and give rise to ferromagnetic contributions.
25. L. Néel, *Ann. Phys. (Paris)* **3**, 137 (1948).
26. We prepared $K_4[V(CN)_6]$ by adding a solution of KCN (2.56 g, 39.4 mmol) in water (60 ml) to a solution of $V(H_2O)_6(OSO_2CF_3)_2$ (*36*) (1.50 g, 3.28 mmol) in water (25 ml) under argon. The dark brown solution was brought to reflux for 30 min and then was taken to dryness under vacuum. The resulting yellow solid was washed with methanol (30 ml) and extracted into an aqueous 3.5 M KCN solution (70 ml). The orange-yellow extract was filtered, reduced in volume to saturation (~25 ml), and cooled to 5°C to afford orange needles of $K_4[V(CN)_6]$. The yield was 0.66 g (55%).
27. We prepared $(NEt_4)_4[V(CN)_6]$ by adding a solution of $(NEt_4)CN$ (1.37 g, 8.75 mmol) in acetonitrile (30 ml) to a solution of $V(H_2O)_6(OSO_2CF_3)_2$ (*36*) (0.50 g, 1.1 mmol) in acetonitrile (26 ml) under argon. The dark brown solution was brought to reflux for 30 min, filtered, reduced in volume to saturation (~20 ml), and cooled to −20°C to afford a brown solid. The crude product was collected by filtration and dissolved in a solution of $(NEt_4)CN$ (1.12 g, 72 mmol) in acetonitrile (60 ml). The resulting red-brown solution was brought to reflux for 5 min, filtered, concentrated to ~20 ml, and cooled to −20°C to afford $(NEt_4)_4[V(CN)_6]$ as a brown solid. The yield was 0.17 g (21%).
28. N. E. Dixon, G. A. Lawrance, P. A. Lay, A. M. Sargeson, H. Taube, *Inorg. Synth.* **24**, 243 (1986).
29. Calculated composition for $C_6N_6Cs_2MnV$ (**1**): C, 13.6%; N, 15.9%; Mn, 10.4%; V, 9.65%. Found: C, 13.7%; N, 16.1%; Mn, 11.6%; V, 10.2%. Calculated composition for $C_9H_{13}Mn_{1.25}N_{5.5}O_2V$ (**2**): C, 30.8%; H, 4.02%; N, 21.9%; Mn, 19.6%; V, 14.5%. Found: C, 30.0%; H, 4.19%; N, 18.2%; Mn, 20.8%; V, 14.8%. Discussions of alternative formulations for **2** such as $(Et_4N)_{0.5}Mn_{1.25}[V(CN)_4(OH)]\cdot H_2O$ await additional data.
30. E. Reguera, J. F. Bertrán, L. Nuñez, *Polyhedron* **13**, 1619 (1994).
31. J. S. Smart, *Am. J. Phys.* **23**, 356 (1955).
32. The saturation magnetization was calculated from the formula $M = g\mu_B N_A S$, where μ_B is the Bohr magneton, N_A is Avogadro's number, and S is the net spin per formula unit. The Landé g factor was assumed to be equal to 2 for both metal centers.
33. Further support for a large local antiferromagnetic interaction between the V^{II} and Mn^{II} spin centers in **2** comes from the χT value of 6.1(2) cm^3 K mol^{-1} at 350 K, which is smaller than the value of 7.4 cm^3 K mol^{-1} calculated for a thermally random array of Mn^{II} (S = 5/2) and V^{II} (S = 3/2) spin centers in a 1.25 to 1 ratio.
34. In contrast, the ferrimagnetic Cr-based Prussian blue analogs $[Cr_5(CN)_{12}]\cdot 10H_2O$ and $Cs_{0.75}$ $[Cr_{2.125}(CN)_6]\cdot 5H_2O$, which have T_N of 240 and 190 K, respectively, exhibit minima in their curves of χT versus T below 300 K (*18*). The absence of such a minimum for **2** suggests that its exchange interactions are stronger than in these cyanochromates.
35. The remnant magnetizations for **1** and **2** are ~1.95 × 10^3 G cm^3 mol^{-1} at 10 K and ~1.39 × 10^3 G cm^3 mol^{-1} at 50 K, respectively.
36. D. G. L. Holt, L. F. Larkworthy, D. C. Povey, G. W. Smith, G. J. Leigh, *Inorg. Chim. Acta* **169**, 201 (1990).
37. This work was supported by the Department of Energy. The work of W.R.E. was supported by a fellowship from the Department of Chemistry. We thank C. Treadway for valuable assistance. We thank M. Rosenblatt, D. White, and K. S. Suslick for assistance with Fig. 1.

4 October 1994; accepted 30 December 1994

Orientational and Magnetic Ordering of Buckyballs in TDAE-C_{60}

D. Mihailovic, D. Arcon, P. Venturini, R. Blinc,
A. Omerzu, P. Cevc

Spin ordering in the low-temperature magnetic phase is directly linked to the orientational ordering of C_{60} molecules in organically doped fullerene derivatives. Electron spin resonance and alternating current susceptometry measurements on tetrakis(dimethylamino)ethylene-C_{60} (TDAE-C_{60}) (Curie temperature T_c = 16 kelvin) show a direct coupling between spin and merohedral degrees of freedom. This coupling was experimentally demonstrated by showing that ordering the spins in the magnetic phase imprints a merohedral order on the solid or, conversely, that merohedrally ordering the C_{60} molecules influences the spin order at low temperature. The merohedral disorder gives rise to a distribution of π-electron exchange interactions between spins on neighboring C_{60} molecules, suggesting a microscopic origin for the observed spin-glass behavior of the magnetic state.

Soon after the discovery by Krätschmer *et al.* (*1*) of an efficient synthesis route for C_{60}, an organic magnetic material based on C_{60} was reported (*2*). The material, which is essentially C_{60} doped with the organic donor TDAE, showed a transition to a magnetic state at a temperature of 16.1 K. This discovery sparked a series of investigations, some aiming to find new organic magnetic materials based on fullerenes. As a result, systematic investigations provided a good phenomenological account of the magnetic properties of such materials. They appeared to be described well by a spin-glass model (*3*) with a nonzero local field (*4*), although alternative suggestions of superparamagnetism (*5*) and itinerant ferromagnetism (*2*) have also been proposed. In addition, two similar materials have now been synthesized with different donors and C_{60}-derived acceptor molecules exhibiting a cusp in the low-temperature static spin susceptibility similar to that of TDAE-C_{60}: cobaltocene-doped dinitro-spiromethano-fullerene ($T_c \approx$ 8 K) (*6*) and cobaltocene-doped 3-nitrophenyl C_{61} ($T_c \approx$ 30 K) (*7*). In spite of this, the microscopic origin of the glassy behavior remained a mystery until now.

Here we report the discovery of a direct link between the buckyball orientational (merohedral) order and the spin order. We suggest that the exchange interaction between π-electrons on neighboring C_{60} molecules is responsible for the spin-spin interaction and that the glassy behavior is a direct consequence of the inherent merohedral disorder. By externally manipulating the degree of fullerene molecular order, we are able to tune T_c, the temperature of the low-temperature magnetic transition, in effect changing the spin ordering through manipulation of the exchange interaction between spins on the fullerene molecules.

Our synthesis of the stoichiometric TDAE-C_{60} compound followed the standard route (*2*), resulting in a 1:1 ratio of TDAE and C_{60} in a solid with a monoclinic C2 structure, which is similar to the usual cubic symmetry of C_{60} but the unit cell has correspondingly smaller inter-

---

Jozef Stefan Institute, Jamova 39, Ljubljana, Slovenia.